

**The Kröhnke synthesis of benzo[a]indolizines revisited:
towards small, red light emitters**

Journal:	<i>Organic Chemistry Frontiers</i>
Manuscript ID	QO-RES-01-2022-000097.R1
Article Type:	Research Article
Date Submitted by the Author:	09-Feb-2022
Complete List of Authors:	Badaro, Jaqueline; Institute of Organic Chemistry PAS, Koszarna, Beata; Polish Academy of Sciences Bousquet, Manon; Université de Nantes, CEISAM - UMR 6230 Ouellette, Erik; University of California, Department of Chemistry Jacquemin, Denis; Université de Nantes, CEISAM - UMR 6230 Gryko, Daniel; Polska Akademia Nauk Instytut Chemii Organicznej,

ARTICLE

The Kröhnke synthesis of benzo[*a*]indolizines revisited: towards small, red light emitters

Received 00th January 20xx,
Accepted 00th January 20xx

Jaqueline S. A. Badaro,^a Beata Koszarna,^a Manon H. E. Bousquet,^b Erik T. Ouellette,^{c,d} Denis Jacquemin,^{*b} and Daniel T. Gryko,^{*a}

DOI: 10.1039/x0xx00000x

Benzo[*a*]indolizines with an ordered arrangement of various electron-withdrawing substituents (NO₂, CF₃, CN, CO₂R and COPh) were prepared directly from pyridinium salts and chloronitroarenes, allowing for refined control of the photophysical properties. Facile entry into almost unknown isoindolo[1,2-*a*]isoquinolines is disclosed to demonstrate the potential of this method. The rational manipulation of the substituents makes it possible to obtain electron-deficient dyes (HOMO ≈ -5.6 eV) with yellow, orange to red emission, large Stokes shifts (up to 9000 cm⁻¹) and fluorescence quantum yields reaching 0.58. Strong emission in spite of the presence of an NO₂ group has been rationalized by a large singlet-triplet energy gap combined with small spin-orbit couplings, hence small intersystem crossing. The ability to substitute various electron-withdrawing groups at multiple positions on this heterocyclic skeleton offers an unprecedented opportunity to study their effect on the fate of the molecules in the excited state.

Introduction

Indolizines, although known since the 19th century,^{1–4} have always been overshadowed by regioisomeric indoles. Only during the last two decades was their chemistry rejuvenated, likely because of their potential as fluorophores,^{5–11} which is especially strong for π-expanded indolizines. In recent years, multiple new methods for indolizine synthesis have been revealed,^{12–14,14–19} nicely complementing older approaches.^{20–24} There are a few basic classes of benzoindolizines: pyrrolo[1,2-*a*]quinolines,^{25–36} pyrrolo[2,1-*a*]isoquinoline,^{37–40} benzo[*b*]indolizine^{41–48} and benzo[*a*]indolizines (pyrido[2,1-*a*]isoindoles)^{49–61} (Fig. 1). The latter ones attracted our particular attention since they are considered as π-expanded isoindoles, which are rarely encountered. However, benzo[*a*]indolizines are reported to be very unstable under ambient conditions.⁴⁹ To overcome this instability issue, adding several electron-withdrawing groups (EWGs) could be an advantageous strategy. At the same time, the presence of electron-withdrawing groups would polarize the π-system and induce bathochromic shifts in both the absorption and emission spectra.⁶² Taking this into account, we reasoned that a one-pot reaction with the potential to assemble a π-expanded indolizine core decorated with several EWGs would be an appreciated

addition to the existing repertoire of benzo[*a*]indolizines synthetic methodologies. Inspired by a LEGO™-type philosophy, our target strategy was to build a final scaffold from easily available building blocks.

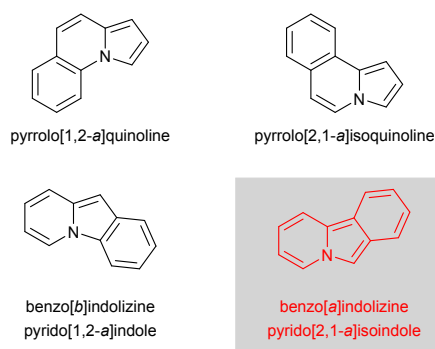


Fig. 1 Structures of various benzoindolizines.

In light of all these requirements, we identified the Kröhnke method for the synthesis of benzo[*a*]indolizines from pyridines, ω-bromoacetophenones, and picryl chloride (Scheme 1)^{52,63,64} as the most promising starting point. This methodology consists of three steps: (1) quaternization of pyridine with (Hal)CH₂(EWG) reagents; (2) C-arylation of the resulting pyridinium salts with 1-chloro-2,4,6-trinitrobenzene; and (3) final 1,5-electrocyclization forming a five-membered central ring. The mechanism of the last key step relies on the formation of vinylpyridinium ylides which are prone toward 1,5-electrocyclization.^{65,66} The initially formed dihydroindolizine eliminates NO₂⁻ and furnishes the final aromatic product. The trouble with Kröhnke's approach is that it is mostly limited to explosive 1-chloro-2,4,6-trinitrobenzene. The intriguing feature, however, is that authors consistently reported strong

^a Institute of Organic Chemistry, Polish Academy of Sciences, Kasprzaka 44/52, 01-224 Warsaw, Poland. E-mail: dtgryko@icho.edu.pl

^b CEISAM Lab—UMR 6230, CNRS, University of Nantes, Nantes, France. E-mail: Denis.Jacquemin@univ-nantes.fr

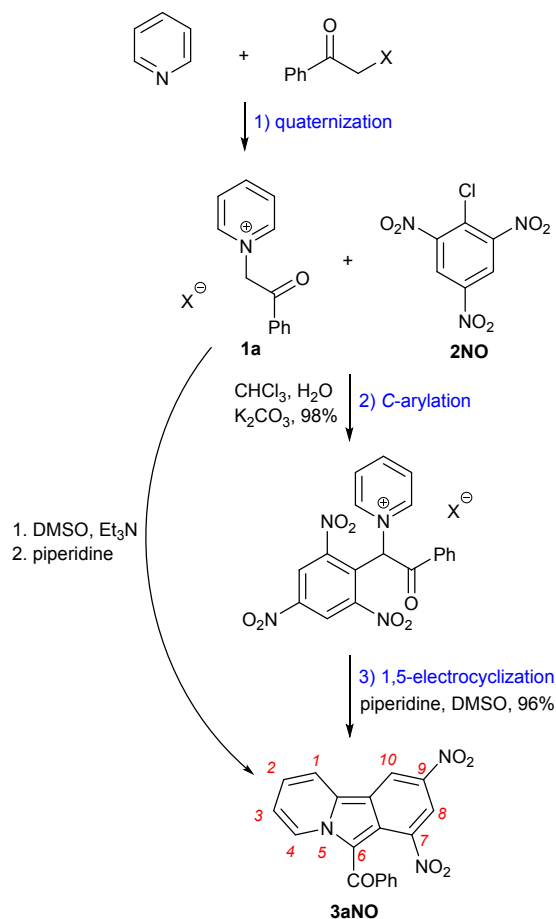
^c Department of Chemistry, University of California, Berkeley, 420 Latimer Hall, Berkeley, CA, USA.

^d Chemical Sciences Division, Lawrence Berkeley National Laboratory, 1 Cyclotron Road, Berkeley, CA, USA.

Electronic Supplementary Information (ESI) available: synthetic optimization studies, crystallographic data, electrochemical and computational details, copies of NMR spectra. See DOI: 10.1039/x0xx00000x

red fluorescence for the resulting nitro-derivatives, which is both rare^{67,68} and worth exploring. In addition, given that almost all published derivatives possess a PhCO at position 6, which typically leads to fluorescence quenching due to enhanced intersystem crossing, the observed emission is even more perplexing. Having all these aspects in mind we conceived a journey aiming at exploring this methodology, expanding the scope, and revisiting the emissive properties of benzo[*a*]indolizine.

decreased reactivity of chloroarenes **2CN** and **2CF** relative to **2NO**. However, these benzo[*a*]indolizines featuring a PhCO group at position 6 possessed rather weak fluorescence, most plausibly due to the presence of the carbonyl group (*vide infra*). Thus, we decided to replace the C=O with the CN group at position 6 and we synthesized dye **3cCF**, aiming at stronger emission intensity. Novel benzo[*a*]indolizine **3cCF** indeed possessed a visibly stronger fluorescence and was used as a model for synthetic optimization studies (see ESI for details).



Scheme 1 The Kröhnke method for the benzo[*a*]indolizine synthesis.

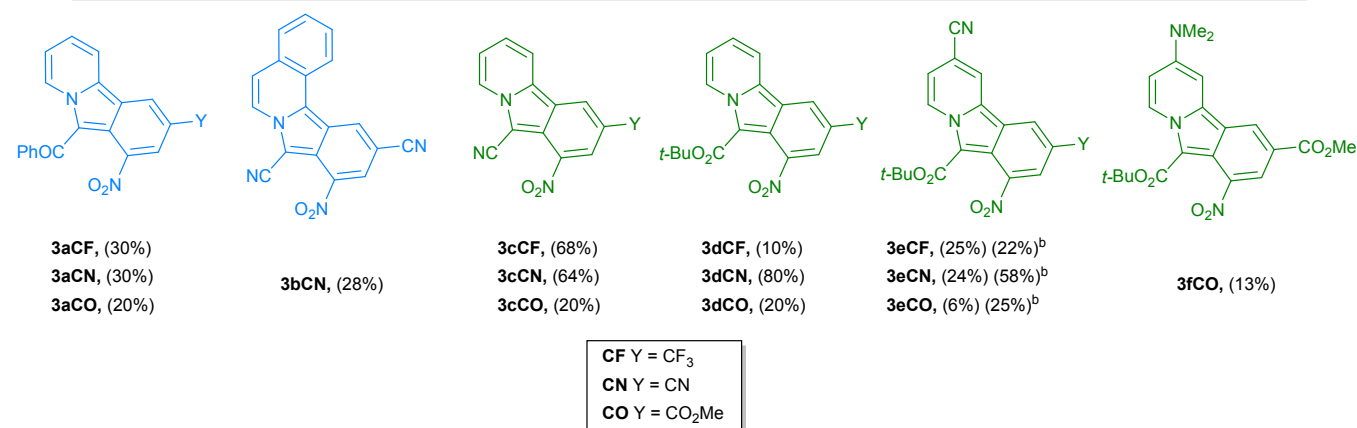
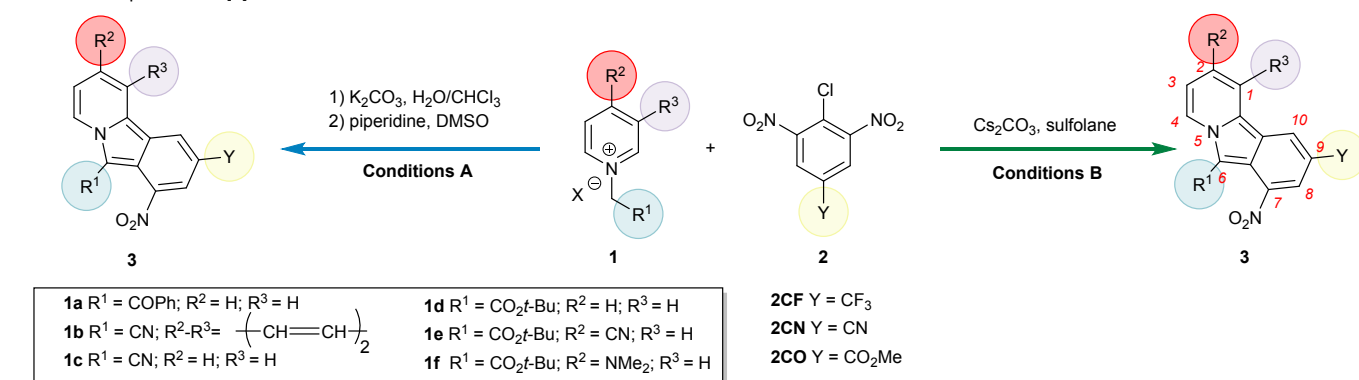
Results and Discussion

Synthesis. Our investigation started from the synthesis of benzoindolizines **3aCF**, **3aCN** and **3aCO** (Scheme 2) following the method developed by Augstein and Kröhnke in 1967 (conditions A).⁵² We found that these three heterocycles could be prepared under the conditions originally published for **3aNO** (i.e. C-arylation in CHCl₃/H₂O/K₂CO₃ system followed by 1,5-electrocyclization mediated by piperidine, Scheme 1) in yields ranging from 20% to 30%. Lower yields may originate from the

Having established the optimal reaction conditions (Cs₂CO₃, sulfolane, RT, 16 h), the substrate scope of benzo[*a*]indolizine synthesis was evaluated. As shown in Scheme 2, various pyridinium salts, as well as an isoquinolinium salt reacted with different 4-chloro-3,5-dinitrobenzenes, successfully giving the products that exhibited different combinations of groups at positions 6 (R¹), 9 (Y), and 2 (R²). The presence of CO₂Me as Y led to lower yields of the final products (**3aCO**, **3cCO**, and **3dCO**), but what dramatically compromised the success of the reaction was the presence of a substituent R². The tested building blocks possessing only one NO₂ at position *ortho* to Cl, such as 1-chloro-2,4-dinitro-6-trifluoromethylbenzene or 2-chloro-3,5-dinitropyridine, were found to be inefficient. A similar outcome was observed for chloroarenes possessing less activated C-Hal bond such as 2,4-dinitrofluorobenzene or 2,4-dichloro-1,5-dinitrobenzene. This evidence suggests that it is mandatory to have two NO₂ in *ortho* positions to the halogen atom for the reaction to proceed to completion.

In the course of this scope investigation, it was noted that quaternary salts derived from pyridines substituted at position 4 with an electron-withdrawing group, such as CN (**3eCF**, **3eCN**, and **3eCO**), were less reactive than the salts **3a**, **3c** and **3d** derived from unsubstituted pyridine. In fact, a four-fold decrease in the yield was observed, with the exception of **3eCF**. Similarly, the presence of an electron-donating group such as NMe₂ (**3fCO**) decreased the product yield from 20% to 13%. Furthermore, further expanding the scope, i.e., starting from 4-methoxypyridine and 4-trifluoromethylpyridine, was unsuccessful. Consequently, another optimization study (see ESI for details), was conducted using **3eCN** as a model which enabled to identify *tert*-butylimino-tri(pyrrolidino) phosphorane (BTPP) as the suitable base (the yield of **3eCN** was increased to 58%).

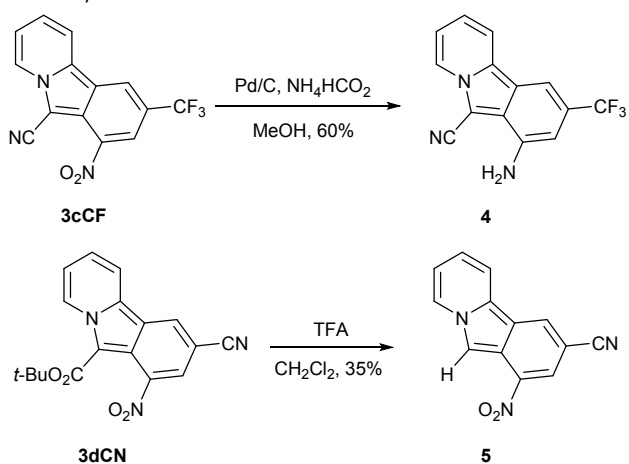
The novel reaction conditions (BTPP, DMSO, RT, 16 h) were then tested for the synthesis of other benzo[*a*]indolizines from salt **1e**. It turned out, however, that yields of dyes **3eCF** and **3eCO** were considerably lower, and the efficiency of the reactions starting from quaternary salts derived from unsubstituted pyridine were below 5% (Scheme 2).

Scheme 2 Scope of benzo[*a*]indolizines^a

^a Structures of products obtained according to conditions A (blue) or B (green)

^b Yields obtained according to the best condition of the second optimization study (BTTP as base and DMSO as solvent).

Scheme 3 Synthesis of 4 and 5 from 3cCF and 3dCN



The obtained benzo[*a*]indolizines offer significant synthetic possibilities due to the presence of several functional groups. In order to explore these possibilities two additional derivatives (**4** and **5**) were obtained via transformations of **3cCF** and **3dCN**, respectively (Scheme 3). The former was obtained thanks to the reduction of the nitro group to an amine, catalyzed by Pd/C with ammonium formate as the proton source.⁶⁹ The latter resulted from the removal of CO_2t-Bu in a reverse Friedel-Crafts⁷⁰ reaction with TFA as a source of proton and acidic species.

Single-Crystal X-ray diffraction study. To date, only a handful of synthetic procedures were developed affording an isoindolo[1,2-*a*]isoquinoline core^{52,55,59,60,71} and to demonstrate that we have successfully obtained compound **3bCN** possessing the expected geometry, single-crystal X-ray diffraction studies were performed (Fig. 2). The crystal for analysis was obtained from the slow diffusion of diethylether into a DMF solution and data obtained show us that the structure is planar and belongs to the P2(1)/n space group within the monoclinic crystal system (for further information see SI). Note that the CN at position 6 is slightly deformed from linearity to accommodate for the vicinal nitro group.

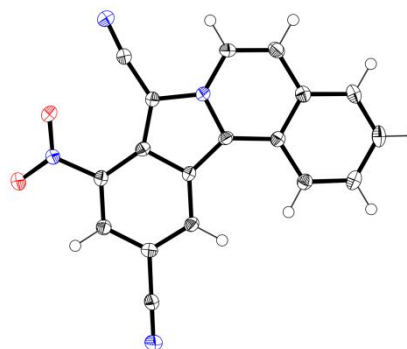


Fig. 2 Crystallographic structure of dye **3bCN**.

Photophysical properties. The UV-VIS absorption and emission spectra were recorded in DCM and toluene for all dyes, and the related data are collected in Table 1. A comparison between the photophysical parameters and those available for parent benzo[*a*]indolizine (fluorescence quantum yield = 14 % in DCM, with $\lambda_{\text{abs}} = 368$ nm and $\lambda_{\text{em}} = 498$ nm)⁷² reveals a significant bathochromic shift of both absorption and emission spectra for the novel highly polarized benzo[*a*]indolizines. The λ_{abs} of the vast majority of the obtained dyes are located within 400-500 nm range. Emission is typically in the yellow-orange-red region of the visible spectral range and the related fluorescence quantum yield (Φ_{fl}) varies from 0.6 to hardly detectable level. The presence of an electron-donating NMe₂ group (**3fCO**) led to the strongest bathochromic shift, especially in the case of emission ($\lambda_{\text{em}} = 832$ nm in DCM). Significant solvatochromism of both absorption and emission, as well as a clear trend of decreasing Φ_{fl} while moving from toluene to DCM for all compounds, clearly point to marked intramolecular charge transfer character (ICT). Comparisons between some representative benzo[*a*]indolizines are displayed in Fig. 3a-3c.

There are a few clear trends. According to expectations the fluorescence strength is weak (≈ 0.1) in the *3a series* where all dyes possess a PhCO group. The strongest emission ($\Phi_{\text{fl}} \approx 0.5$) has been observed for dyes bearing a CN group at position 6 (i.e. *3c series*, **3bCN** and **4**). Fluorescence is weaker in the *3d series* and *3e series*, although they do not have a keto group at position 6 ($\Phi_{\text{fl}} \approx 0.1-0.2$). The presence of an additional CN group at position 2 improves emission intensity (*3d series* versus *3e series*). The reasons for these complex behaviours were rationalized by first principles calculations (*vide infra*).

The broad comparison of photophysical properties reveals that that the substituent at position 6 and not the one in position 9 has a major influence. Indeed, the difference in the electronic character of the groups in position 6 influences the λ_{abs} . If a CN group is there (**3cCO**), $\lambda_{\text{abs}} = 481$ nm i.e. it is red-shifted compared to the other benzo[*a*]indolizines possessing a CO₂Me group at position 9 ($\lambda_{\text{abs}} = 404-446$ nm) (Fig. 3a). Still, in the *3a series*, the strength of an electron-withdrawing group at position 9 also contributes to a moderate bathochromic shift. The presence of an additional benzene ring (**3bCN** vs. **3cCN**) has a limited effect on photophysical properties. Adding a CN group at position 2 causes hypsochromic shift of both absorption and emission (**3dCN** vs. **3eCN**).

Table 1 Photophysical data of synthesized benzo[*a*]indolizines

Cpd	Solv	λ_{abs} [nm]	λ_{em} [nm]	$\Delta\bar{\nu}$ [cm ⁻¹]	ϵ [M ⁻¹ cm ⁻¹]	Φ_{fl}
3aCF^a	DCM	475	704	6800	5000	0.02
	Tol	468	644	5800	5600	0.09
3aCN^a	DCM	480	687	6300	4600	0.03
	Tol	471	641	5600	4500	0.10
3aCO^a	DCM	461	681	7000	4500	0.03

3bCN^a	Tol	415	630	4600	4600	0.24
	DCM	494	616	4000	11000	0.40
3cCF^a	Tol	490	574	3000	7200	0.58
	DCM	488	603	3900	8000	0.38
3cCN^a	Tol	483	569	3100	5900	0.58
	DCM	490	601	3800	8800	0.38
3cCO^a	Tol	486	569	3000	7600	0.53
	DCM	482	597	4000	5600	0.45
3dCF^b	Tol	481	557	2800	6300	0.58
	DCM	452	685	7500	11800	0.02
3dCN^b	Tol	449	618	6100	10500	0.09
	DCM	457	674	7000	6000	0.03
3dCO^b	Tol	451	622	6100	5700	0.10
	DCM	449	664	7200	5800	0.03
3eCF^b	Tol	446	616	6200	5400	0.13
	DCM	447	629	6500	31000	0.17
3eCN^b	Tol	448	596	5500	25000	0.20
	DCM	400	628	9100	16000	0.16
3eCO^b	Tol	402	585	7800	14000	0.20
	DCM	404	617	8500	14000	0.22
3fCO^a	Tol	415	575	6700	12000	0.24
	DCM	510	832	7600	5000	<0.001
4^c	Tol	504	721	6000	5300	0.01
	DCM	377	495	6300	13000	0.26
5^d	Tol	378	495	6300	13000	0.20
	DCM	549	677	3400	6900	0.04
	Tol	529	635	3200	5000	0.11

^a Fluorescence quantum yield measured with Fluorescein in 0.1 M aqueous solution of NaOH ($\Phi_{\text{fl}}=0.79$) as reference.

^b Fluorescence quantum yield measured with Coumarin 153 in ethanol ($\Phi_{\text{fl}}=0.38$) as reference.

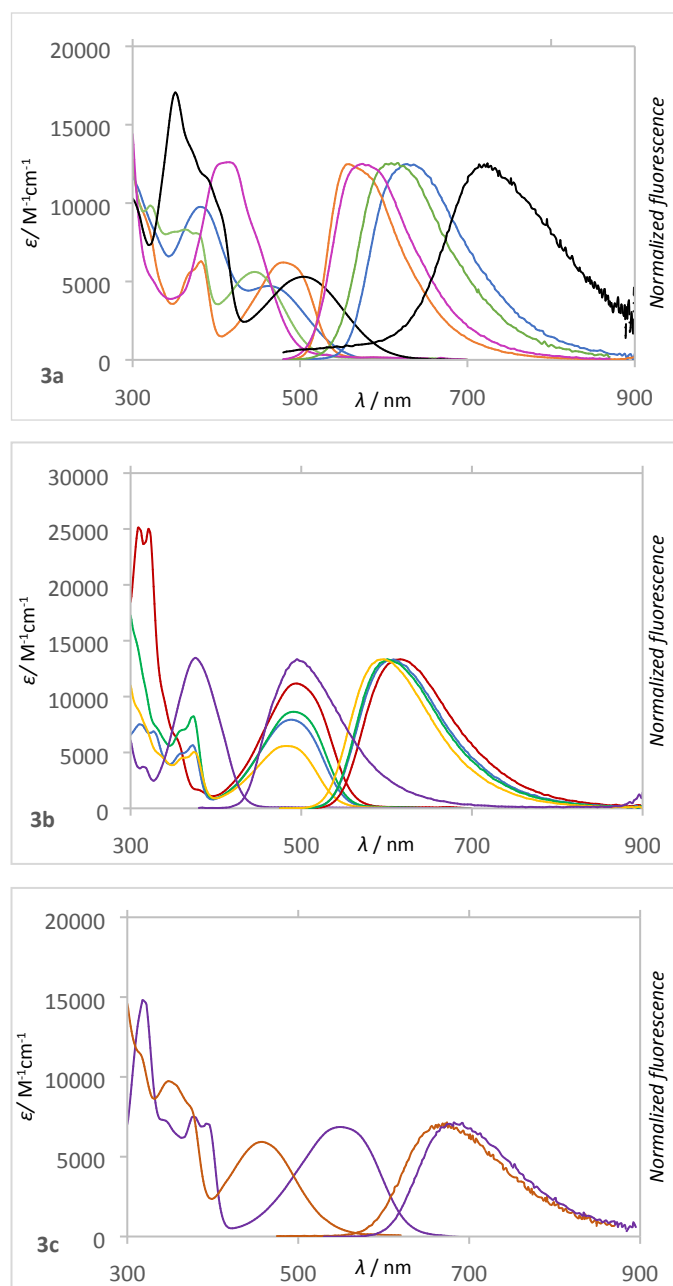
^c Fluorescence quantum yield measured with 9,10-diphenylanthracene in cyclohexane ($\Phi_{\text{fl}}=1$) as reference.

^d Fluorescence quantum yield measured with Sulforhodamine 101 in ethanol ($\Phi_{\text{fl}}=0.9$) as reference.

Interestingly truncating an electron-withdrawing ester group at position 6 (**3dCN** vs. dye **5**) causes a bathochromic shift of absorption (≈ 100 nm in DCM) but not of emission (Fig. 3c). The presence of a CO₂*t*-Bu group also increases the Stokes shift ($\Delta\bar{\nu}$) from 5000 cm⁻¹ to 5700 cm⁻¹. For both dyes, Φ_{fl} is small (only 0.10 and 0.11 in toluene), but **5** is also unstable, decomposing only a few seconds after irradiation.

It is clear that the presence of NO₂ at position 7 controls the photophysics of these dyes. Its replacement with electron-donating NH₂ (compound **4**) causes marked hypsochromic shift of both absorption and fluorescence (Fig. 3b, purple curve). Furthermore, in contrast to what was expected, the absence of NO₂ did not increase the fluorescence yield, instead it decreased by almost a third (0.38 and 0.26, respectively).

Fig. 3. Absorption and emission spectra of the representative benzo[*a*]indolizines in DCM and toluene.



3a Molar absorptivity (solid line) and normalized emission (discontinued line) spectra of **3aCO**, **3cCO**, **3dCO**, **3eCO**, and **3fCO** (blue, orange, green, pink, black) in toluene

3b Molar absorptivity (solid line) and normalized emission (dashed line) spectra of **3dCN**, **3cCF**, **3cCN**, **3cCO**, **4** (red, blue, green, orange, purple) in DCM.

3c Molar absorptivity (solid line) and normalized emission (dashed line) spectra of **3dCN** (orange) and **5** (purple) in DCM.

Theoretical analysis. We have performed theoretical calculations (see computational details) to understand the unusual photophysical properties of the synthesized compounds. All calculations were made using DCM as solvent. First, in Fig. 4, we show density difference plots for selected compounds. In all structures, it is clear that the nitro group at position 7, the strongest EWG group acts as an accepting group (mostly in red),

whereas the five-membered ring acts as the main electron-rich moiety (main in blue). Equally interesting is that the substituent at position 9 plays a limited role in the excited state. This is consistent with the data listed in Table 1 that show similar values in a given series of compounds (e.g., **3aCF**, **3aCN**, and **3aCO** have similar absorption spectra). What is even more valuable is that the substituents at position 6, either CPh, CO₂t-Bu, or even CN appear to play the role of a secondary donor (see **3bCN** in Fig. 4 for example). Interestingly, according to computational studies, replacement of CN with a bulkier group at position 6 induces significant twisting of the structure, including of the nitro group (see **3cCN**→**3eCN**, in Fig. S3 of the SI).

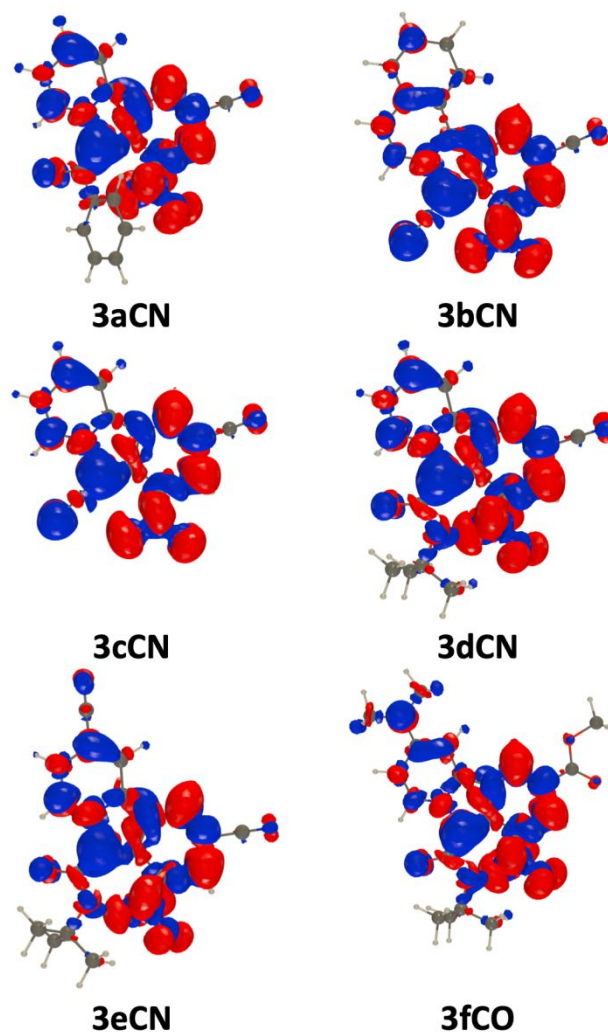


Fig. 4 Density difference plots for selected compounds. Blue and red lobes correspond to zones of decrease and increase of electron density upon absorption. Contour: 8×10^{-4} .

To allow for more quantitative comparisons between theory and experiment, we have computed the excited-state properties, which are summarized in Table 2. First, let us note that the trends in both vertical absorption and emission wavelengths nicely follow their experimental counterparts with

$R=0.91$ for both properties. Nevertheless, to allow more physically well-grounded comparisons, we have also determined 0-0 energies for all compounds. These values, which include the difference of zero-point vibrational energy (ZPVE) between the two states, can be compared directly to the absorption/emission crossing point. The mean absolute error (MAE) obtained by such comparison is 0.12 eV, a value typical of excited state calculations performed at the CC2 level.⁷³ The correlation coefficient is 0.92. These data indicate that the selected level of theory is well suited to investigate this specific class of compounds. In Table 2, we report the ICT parameters as obtained by Le Bahers' model.⁷⁴ As expected, and consistent with the experimental solvatochromic effects, we note significant ICT (except in **4**), the largest effect being the displacement of 0.73 e over 2.05 Å (**3fCO**), large values for rather compact dyes.⁷⁴ In a given series, it is the CF₃ that induces the strongest ICT and not the CN, consistent with the topology of the excited states in Fig. 4 indicating that the accepting groups at position 9 do not strongly impact the topology of the excited states.

Table 2 Computed photophysical data in DCM for all benzo[*a*]indolizines: vertical absorption and emission (in nm), 0-0 energies (in eV), ICT distance and charge (in Å and e, respectively). Fluorescence quantum yields computed on the basis of radiative rates and internal conversion rates only. Singlet-triplet gaps (at the S₁ geometry, eV) and spin-orbit coupling between the S and T states (cm⁻¹) at that same geometry.

Cpd	λ_{abs} [nm]	λ_{em} [nm]	ΔE_{00} [eV]	d^{CT} [Å]	q^{CT} [e]	Φ_{fl}	ΔE_{ST} [eV]	SOC [cm ⁻¹]
3aCF	440	639	2.07	2.04	0.75	0.21	0.26	0.14
3aCN	447	634	2.08	1.88	0.71	0.22	0.23	0.10
3aCO	439	619	2.11	1.97	0.72	0.24	0.25	0.16
3bCN	448	551	2.22	1.89	0.66	0.45	0.44	0.02
3cCF	447	547	2.26	2.11	0.70	0.43	0.33	0.04
3cCN	452	546	2.25	1.91	0.67	0.45	0.31	0.01
3cCO	443	531	2.31	1.98	0.67	0.49	0.34	0.01
3dCF	426	621	2.14	1.92	0.72	0.25	0.28	0.20
3dCN	434	617	2.13	1.76	0.69	0.24	0.27	0.16
3dCO	425	599	2.19	1.82	0.69	0.29	0.29	0.19
3eCF	406	564	2.30	1.97	0.65	0.43	0.44	0.13
3eCN	414	559	2.30	1.81	0.61	0.45	0.43	0.09
3eCO	406	541	2.36	1.79	0.60	0.51	0.47	0.11
3fCO	504	768	1.79	2.05	0.73	0.12	0.16	0.13
4^a	353	425	2.96	0.91	0.42	0.66	0.21	0.04
5	492	608	2.04	2.00	0.65	0.26	0.35	0.01

^a S-T gaps with the second and not first triplet state.

Certainly, more intriguing are the rather good emissive properties of some of the dyes. We have therefore put efforts into the simulations of the quantum yield of emission of all compounds. Within the TCVF formalism (see computational details),⁷⁵ it is possible to have a uniform description of the radiative (k_r) and internal conversion rates (k_{ic}) from first-principle calculations of the vibronic couplings, and hence to deduce a theoretical Φ_{fl} , but such a computed yield total neglects all other non-radiative pathways. Considering the nitro-bearing dyes have a quite rigid core, the likely competitive non-radiative pathway is intersystem crossing (ISC) to the triplet

state, a phenomenon typically invoked to explain the quenching of emission in nitro derivatives.^{62,59} The theoretical values of Φ_{fl} determined neglecting ISC should therefore be equal (if ISC is negligible) or larger (if ISC is significant) than their experimental counterparts. This is exactly what is found when comparing Tables 1 and 2. For **3bCN**, **3cCF**, **3cCN**, and **3cCO**, the computed and measured values are very nicely matching (ca. 40%), the trends in the series being equivalent in both theory and experiment.

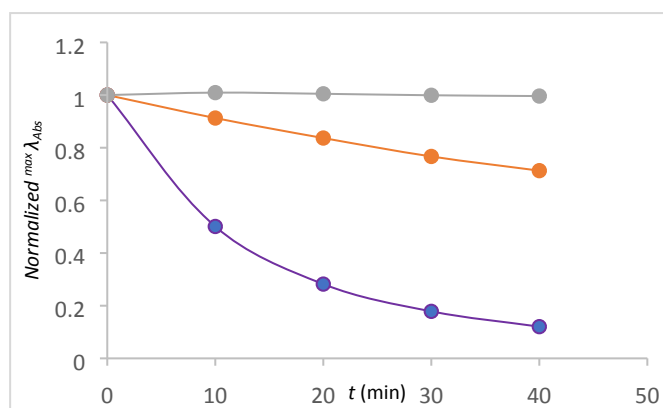
Consistently, for these four compounds, the singlet-triplet gaps determined at the excited-state geometry are large (>0.3 eV), and the spin-orbit coupling elements are totally negligible (<0.05 cm⁻¹), indicating trifling ISC. In other words, theory indicates that the $\Phi_{fl} \approx 40\%$ measured in DCM is related to the vibrational and electronic structure of the dyes and is not perturbed by other factors (electron transfer, TICT, ISC, etc.). Let us now turn towards the *3e series*, for which the computed Φ_{fl} remains similar to the one of *3c series*, but the experimental values have dropped by a factor of 2 (to ca. 20%). In this case, while the computed S-T gap remains large, the SOC are notably increased (≈ 0.10 cm⁻¹), indicating that ISC might start playing a role in decreasing the yields. For the compounds in both *3a series* and *3d series*, as well as **3fCO**, the Φ_{fl} computed on the basis of vibronic couplings are ca. 20%, whereas the emission measured in DCM are very weak (3% at most). However, for all those compounds, one notices rather small S-T gaps (<0.3 eV, even 0.16 eV in **3fCO**) together with SOCs exceeding 0.10 cm⁻¹, indicative of stronger ISC than in the other series. For derivatives of the *3a series* and *3d series*, not only is the ratio between the radiative and internal conversion rates less favourable than in *3c series*, but ISC is also playing a role. This illustrates the challenge of optimizing the fluorescence quantum yield. Finally, **4** is more difficult to analyse because the presence of the NH₂ group makes non-harmonic vibrational effects larger. Additionally, in strong contrast with the other systems, two triplet states are accessible from the lowest singlet in **4**.

Photostability. To examine the photostability of compounds **3dCN** and **4**, their solutions in DCM were exposed to a Xe lamp monitoring the absorption maximum at the appropriate wavelength with respect to the irradiation time (Fig. 4). Comparing both structures with Rhodamine 6G we can see that **4** is much less stable than **3dCN**, but both are visibly less stable than the reference compound (see Fig. 5). During all experiments, the concentration of the former was stable, while after only 10 min of irradiation, the content of **4** decreased by 50%, while the **3dCN** was decreased by 10%. At half of the experiment time, the **3dCN** concentration was around 80% while for **4** it dropped to ca. 30%. After 40 min irradiation, the absorption intensity at the λ_{max} decreased one order of magnitude for **4** but a factor of 3 only for **3dCN**. All of this information is consistent with the expected reactivity of

indolizines.⁷⁶ Structures without substituents at position 6 are very reactive, and the electron density is located in this region, making it a good substrate for electrophilic aromatic substitution.

Electrochemical properties. To investigate the electrochemical properties of exemplary benzo[*a*]indolizines, cyclic voltammetry was conducted in DCM. As shown in Table 3, oxidation events are irreversible for all compounds measured (**3dCN**, **3fCO**, **3aCF**, **3eCN**, **3cCN**). In contrast, the reduction is quasi-reversible for compounds **3dCN**, **3eCN**, and **3cCN**, irreversible for **3aCF**, and reversible for compound **3fCO**. The ionization potentials are similar for all compounds bearing an electron-withdrawing group (CN) in position 2 as well as no substituents.

For compound **3fCO**, possessing an electron-donating group (NMe₂), the ionization potential is lower. The electron affinity is similar for all investigated compounds, hinting that the different substitution patterns have no direct effect on the LUMO energy.



^aPhotostability of **3dCN** (orange) and **4** (purple) in DCM compared to Rhodamine 6G (grey), in EtOH using a collimated light source from a 300W Xe lamp

Conclusions

We reported that the synthesis of benzo[*a*]indolizines from pyridinium salts and derivatives or analogues of 1-chloro-2-nitrobenzene has a reasonable scope and could be used under one-pot protocol to achieve the final dyes in 20-80% overall yields. The presence of up to four different electron-withdrawing groups allowed for studying their impact on desired photophysical properties. The combination of a highly-polarized core and the presence of a nitro group is responsible for yellow to red emission. The nitro group, which often quenches fluorescence to undetectable levels, still gives fluorescence yield of ca. 20-60% for the present dyes, despite its clear participation in the electronic transition. Moderate intramolecular charge transfer which has been introduced to these molecules is strong enough to suppress ISC and weak enough to prevent formation of dark TICT states. The replacement of small electron-withdrawing groups with larger ones at position 6 causes distortion from planarity, which in turn decreases the singlet-triplet energy gap and causes partial fluorescence quenching.

Fig. 5 Photostability of benzo[*a*]indolizines^a

Table 3 Redox potentials measured in dichloromethane^a

Compound	$E_{\text{ox1}}^{\text{pa}}[\text{V}]$	$E_{\text{ox1}}^{\text{onset}}[\text{V}]$	$E_{\text{ox2}}^{\text{pa}}[\text{V}]$	$IP[\text{eV}]$	$E_{\text{red1}}^{\text{pa}}[\text{V}]$	$E_{\text{red1}}^{\text{pc}}[\text{V}]$	$E_{\text{red1}}^{\text{onset}}[\text{V}]$	$E_{\text{red1}}^{1/2}[\text{V}]$	$E_{\text{red2}}^{\text{pc}}[\text{V}]$	$EA[\text{eV}]$
3dCN	1.41	1.30	-	-5.6	-1.1	-0.97	-0.94	-	-1.70	-3.4
3fCO	0.69	0.60	1.22	-4.9	-	-0.94	-0.72	-1.28	-	-3.6
3aCF	1.38	1.24	1.45	-5.6	-0.89	-0.70	-0.85	-	-	-3.5
3eCN	1.67	1.52	-	-5.9	-	-0.92	-0.74	-	-1.63	-3.6
3cCN	1.53	1.43	-	-5.8	-0.8	-0.72	-0.72	-	-1.44	-3.6

^a Measurement conditions: electrolyte (NBu₄ClO₄, c = 0,1M), dry CH₂Cl₂, potential sweep rate: 100 mVs⁻¹, working electrode: glassy carbon (GC), auxiliary electrode: Pt wire, reference electrode: Ag/AgCl; all measurements were conducted at room temperature.

Experimental section

General synthetic information

All reagents and solvents were purchased from commercial sources and used as received. Reactions with moisture and oxygen sensitive compounds were performed under an argon atm. Reaction progress was monitored by means of thin-layer chromatography (TLC), performed on aluminum foil plates, covered with Silica gel 60 F₂₅₄ (Merck). Pure products were achieved by means of column chromatography with silica gel 60 (230–400 mesh). The identity and purity of final products were established by ¹H and ¹³C NMR spectrometry as well as by MS-spectrometry (EI-MS, ESI-MS or APCI-MS). All reported ¹H NMR and ¹³C NMR spectra were recorded on Bruker AM 500 MHz, Varian AM 500 MHz or Varian AM 600 MHz spectrometers. Chemical shifts (ppm) were determined with TMS as internal reference; J values are given in Hz. All melting points were measured with EZ-Melt apparatus.

Salts **1a**⁷⁷, **1b**⁷⁸, **1c**⁷⁹, **1d**⁸⁰, **1e**⁷⁹, and methyl 4-chloro-3,5-dinitrobenzoate (**2O**⁸¹) were synthesized according to previously published procedure, and spectroscopic data are consistent.

1-(2-Oxo-2-phenylethyl)pyridin-1-ium bromide (1a). ¹H NMR (400 MHz, DMSO-d₆) δ 8.98 (d, J = 5.5 Hz, 2H), 8.73 (t, J = 7.8 Hz, 1H), 8.30–8.21 (m, 2H), 8.09–8.03 (m, 2H), 7.78 (d, J = 7.4 Hz, 1H), 7.69–7.61 (m, 2H), 6.47 (s, 2H).

2-(Cyanomethyl)isoquinolin-2-ium chloride (1b). ¹H NMR (500 MHz, DMSO-d₆) δ 10.31 (s, 1H), 8.91 (dd, J = 6.8, 1.3 Hz, 1H), 8.70 (d, J = 6.8 Hz, 1H), 8.60 (d, J = 8.3 Hz, 1H), 8.41 (d, J = 8.2 Hz, 1H), 8.37–8.32 (m, 1H), 8.16–8.11 (m, 1H), 6.22 (s, 2H).

1-(Cyanomethyl)pyridin-1-ium bromide (1c). ¹H NMR (600 MHz, DMSO-d₆) δ 9.25 (d, J = 5.6 Hz, 2H), 8.71 (t, J = 7.8, 1H), 8.26–8.20 (m, 2H), 6.11 (s, 2H).

1-(2-(tert-Butoxy)-2-oxoethyl)pyridin-1-ium bromide (1d). ¹H NMR (500 MHz, CDCl₃) δ 9.43 (d, J = 5.6 Hz, 2H), 8.59 (t, J = 7.8, 1H), 8.16–8.07 (m, 2H), 6.08 (s, 2H), 1.51 (s, 9H).

1-(2-(tert-Butoxy)-2-oxoethyl)-4-cyanopyridin-1-ium chloride (1e). ¹H NMR (500 MHz, DMSO-d₆) δ 9.36 (d, J = 6.5 Hz, 2H), 8.76 (d, J = 6.5 Hz, 2H), 5.68 (s, 2H), 1.45 (s, 9H).

Methyl 4-chloro-3,5-dinitrobenzoate (2CO). ¹H NMR (400 MHz, Chloroform-d) δ 8.59 (s, 2H), 4.02 (s, 3H).

Procedure for the synthesis of 1-(2-(tert-butoxy)-2-oxoethyl)-4-(dimethylamino)pyridin-1-ium chloride (1f). In a round bottom flask under inert atmosphere, 4-(dimethylamino)pyridine (2.44 g, 20 mmol) was mixed together with tert-butyl chloroacetate (2.86 mL, 20 mmol) in neat condition at room temperature. After 30 minutes a light pink

fluffy power started to form. Reaction was stirred for an additional 2.5 hours than the precipitate was filtered off and washed with Et₂O. (3.26 g, 70%); R_f = 0.37 (MeOH/DCM, 1:4) M.p. 178–180°C. ¹H NMR (500 MHz, DMSO-d₆) δ 8.24 (d, J = 7.8 Hz, 2H), 7.07 (d, J = 7.8 Hz, 2H), 5.10 (s, 2H), 3.19 (s, 6H), 1.43 (s, 9H). ¹³C NMR (126 MHz, DMSO-d₆) δ 167.1, 156.5, 143.6, 107.8, 83.3, 57.4, 40.3, 28.2 ppm. HRMS (ESI): m/z calcd for C₁₃H₂₁N₂O₂, 237.1603 [M]⁺; found, 237.1599.

General procedure for the synthesis of benzo[a]indolizines (Condition A)

Salt **1** (2mmol, 1 equiv.) was dissolved in 10 mL of water, 3,5-dinitrobenzoderivative **2** (2 mmol, 1 equiv.) was dissolved in 10 mL of chloroform, and K₂CO₃ (0.552 g, 4 mmol) was dissolved in 5 mL of water. All the solutions were cooled to 0 °C, added in order to a 50 mL round bottom flask and stirred at 0 °C for 30 min. A violet solid, when formed, was filtered. The organic phase containing betaine intermediate was extracted, evaporated, and combined with the solid for the next step. Betaine (2 mmol, 1 equiv.) was dissolved in 6 mL of DMSO at RT. Piperidine (395 mL, 4 mmol) was added and the mixture was stirred for 3 h. The reaction was quenched with a solution of CH₃COOH in H₂O (1:1) and the precipitate was filtered off. The crude product was purified by column chromatography (AcOEt/Hexane, 3:7), unless differently stated.

General procedure for the synthesis of benzo[a]indolizines (Condition B)

In a 50 mL round bottom flask, equipped with magnetic stirrer, pyridinium salt **1** (1 mmol, 1 equiv.) and dinitro-benzo derivative **2** (1 mmol, 1 equiv.) were dissolved in 3 mL of sulfolane. Cs₂CO₃ (1.302 g, 4 mmol) was added, and the reaction mixture was stirred overnight at room temperature. After completion, the reaction was quenched with 3 mL of a solution of CH₃COOH in water (1:1). A precipitate was formed, filtered, and washed with water, unless differently specified. Crude products, when needed, were purified by column chromatography.

7-Nitro-9-(trifluoromethyl)pyrido[2,1-a]isoindol-6-yl(phenyl)methanone (3aCF). According to the general procedure (condition A) 1-(2-oxo-2-phenylethyl)pyridin-1-ium bromide (0.198 g, 1 mmol) and 4-chloro-3,5-dinitrobenzotrifluoride (0.270 g, 1 mmol) were reacted affording **3aCF** (0.110 g, 30%) as orange crystals. R_f = 0.48 (AcOEt/Hexane, 1:2); M.p. 204–206 °C. ¹H NMR (500 MHz, CDCl₃) δ 9.93 (d, J = 7.1, 1H), 8.73 (s, 1H), 8.40 (d, J = 8.7, 1H), 8.33 (s, 1H), 7.69–7.63 (m, 1H), 7.63–7.57 (m, 2H), 7.54–7.45 (m, 2H), 7.45–7.38 (m, 2H). ¹³C NMR (126 MHz, CDCl₃) δ 186.7, 141.4, 140.6, 132.5, 132.4, 129.0, 128.0, 127.6, 125.6, 124.8, 123.5 (q, J = 3.5 Hz), 122.3 (q, J = 3.5 Hz), 121.7, 120.8 (q, J = 34 Hz), 120.3, 120.0, 118.0, 112.9 ppm. HRMS (ESI): m/z calcd for C₂₀H₁₁N₂O₃F₃Na, 407.0619 [M+Na]⁺; found, 407.0625.

6-Benzoyl-7-nitropyrido[2,1-a]isoindole-9-carbonitrile (3aCN). According to the general procedure (condition A) 1-(2-oxo-2-phenylethyl)pyridin-1-ium bromide (0.198 g, 1 mmol) and 4-chloro-3,5-dinitrobenzotrifluoride (0.227 g, 1 mmol) were reacted

affording **3aCN** (0.105 g, 30%) as orange crystals. $R_f = 0.28$ (AcOEt/Hexane, 1:2); M.p. 243–245 °C. $^1\text{H NMR}$ (600 MHz, CDCl_3) δ 9.85 (d, $J = 7.0$ Hz, 1H), 8.78 (s, 1H), 8.39 (d, $J = 8.6$ Hz, 1H), 8.30 (s, 1H), 7.71 (dd, $J = 9.7, 7.8$ Hz, 1H), 7.61 (d, $J = 7.5$ Hz, 2H), 7.53 (dd, $J = 8.3, 7.3$ Hz, 2H), 7.44–7.38 (m, 2H). $^{13}\text{C NMR}$ (126 MHz, CDCl_3) δ 186.8, 171.1, 141.0 (2), 140.3, 132.7, 132.3, 131.0, 129.1, 128.0, 127.8, 127.1, 126.3, 121.1, 120.5, 120.4, 118.2, 118.0, 101.0

HRMS (EI): m/z calcd for $\text{C}_{20}\text{H}_{11}\text{N}_3\text{O}_3$, 341.0800 [M^{+}]; found 341.0797. (Additional solvent peaks are present in NMR spectra and was not possible to remove even after drying overnight)

Methyl 6-benzoyl-7-nitropyrido[2,1- α]isoindole-9-carboxylate (3aCO). According to the general procedure (condition A) 1-(2-oxo-2-phenylethyl)pyridin-1-ium bromide (0.198 g, 1 mmol) and methyl 4-chloro-3,5-dinitrobenzoate (0.260 g, 1 mmol) were reacted affording **3aCO** (0.031 g, 8%) as orange crystals. $R_f = 0.28$ (AcOEt/Hexane, 1:2); M.p. 249–251 °C. $^1\text{H NMR}$ (500 MHz, CDCl_3) δ 9.91 (d, $J = 7.0$ Hz, 1H), 9.18 (s, 1H), 8.74 (s, 1H), 8.41 (d, $J = 8.5$ Hz, 1H), 7.66 (dd, $J = 9.0, 7.8$ Hz, 1H), 7.61 (d, $J = 7.4$ Hz, 2H), 7.53–7.45 (m, 2H), 7.43–7.38 (m, 2H), 4.01 (s, 3H). $^{13}\text{C NMR}$ (126 MHz, CDCl_3) δ 186.8, 165.7, 141.4, 140.1, 133.3, 132.3, 129.0, 128.5, 128.0, 127.7, 126.2, 125.9, 122.4, 120.7, 120.6, 119.8, 118.1, 113.2, 52.6 ppm. HRMS (EI): m/z calcd for $\text{C}_{21}\text{H}_{14}\text{N}_2\text{O}_5$, 374.0903 [M^{+}]; found 374.0907.

9-Nitroisoindolo[1,2- α]isoquinoline-8,11-dicarbonitrile

(3bCN). According to the general procedure (condition A) 1-(cyanomethyl)isoquinolinium chloride (0.338 g, 2 mmol) and 4-chloro-3,5-dinitrobenzotrifluoride (0.454 g, 2 mmol) were reacted affording **3bCN** (0.173 g, 28%) as red crystals after washing with water, MeOH, Et_2O and recrystallized from DMF/ Et_2O . $R_f = 0.45$ (AcOEt/Hexane, 1:1); M.p. 389–391 °C. $^1\text{H NMR}$ (500 MHz, DMF- d_7) δ 10.06 (s, 1H), 9.41 (d, $J = 8.4$ Hz, 1H), 8.96–8.92 (m, 2H), 8.33 (d, $J = 7.9$ Hz, 1H), 8.26 (d, $J = 7.3$ Hz, 1H); missing signal for 2H is probably hid under DMF peak at around 7.9 ppm; crystals were hardly soluble and it was not possible to dissolved them in any standard deuterated solvents. $^{13}\text{C NMR}$ was not possible to record. (APCI): m/z calcd for $\text{C}_{18}\text{H}_8\text{N}_4\text{O}_2$, 312.0647 [M^+]; found 312.0649.

7-Nitro-9-(trifluoromethyl)pyrido[2,1- α]isoindole-6-

carbonitrile (3cCF). According to the general procedure (condition B) *N*-(cyanomethyl)pyridinium bromide (0.119 g, 1 mmol) and 4-chloro-3,5-dinitrobenzotrifluoride (0.270 g, 1 mmol) were reacted, affording **3cCF** (0.192 g, 63%) as orange/red crystals. $R_f = 0.35$ (AcOEt/Hexane, 1:1); M.p. 309–311 °C. $^1\text{H NMR}$ (500 MHz, DMSO- d_6) δ 9.42 (s, 1H), 8.97 (d, $J = 6.6$ Hz, 1H), 8.94 (d, $J = 8.5$ Hz, 1H), 8.65 (s, 1H), 7.92–7.86 (m, 1H), 7.81–7.75 (m, 1H). $^{13}\text{C NMR}$ (126 MHz, DMSO- d_6) δ 136.7, 133.6, 128.3, 127.8, 127.6, 123.1, 122.3, 122.1, 121.2, 120.4, 120.4, 119.6 (q, $J = 36$ Hz), 114.1, 89.1 ppm. HRMS (ESI): m/z calcd for $\text{C}_{14}\text{H}_6\text{F}_3\text{N}_3\text{O}_2\text{Na}$, 328.0310 [$\text{M}+\text{Na}^+$]; found, 328.0315.

7-Nitropyrido[2,1- α]isoindole-6,9-dicarbonitrile (3cCN).

According to the general procedure (condition B) *N*-

(cyanomethyl)pyridinium bromide (0.119 g, 1 mmol) and 4-chloro-3,5-dinitrobenzotrifluoride (0.227 g, 1 mmol) were reacted, affording **3cCN** (0.167 g, 64%) as red crystals. $R_f = 0.25$ (AcOEt/Hexane, 1:1); M.p. 329–331 °C. $^1\text{H NMR}$ (500 MHz, Acetone- d_6) δ 9.38 (d, $J = 1.1$ Hz, 1H), 9.09 (d, $J = 6.7$ Hz, 1H), 8.90 (d, $J = 8.4$ Hz, 1H), 8.85 (d, $J = 1.1$ Hz, 1H), 8.05–7.97 (m, 1H), 7.96–7.91 (m, 1H). $^{13}\text{C NMR}$ (126 MHz, Acetone- d_6) δ 205.2, 133.6, 133.2, 132.4, 128.3, 128.0, 127.1, 121.8, 121.5, 121.0, 119.6, 117.7, 112.8, 101.4 ppm. HRMS (APCI): m/z calcd for $\text{C}_{14}\text{H}_6\text{N}_4\text{O}_2$, 262.0491 [M^+]; found, 262.0498.

Methyl 6-cyano-7-nitropyrido[2,1- α]isoindole-9-carboxylate

(3cCO). According to the general procedure (condition B) *N*-(cyanomethyl)pyridinium bromide (0.119 g, 1 mmol) and methyl 4-chloro-3,5-dinitrobenzoate (0.260 g, 1 mmol) were reacted, affording **3cCO** (0.062 g, 20%) as orange crystals. $R_f = 0.45$ (AcOEt/Hexane, 2:1); M.p. 312–314 °C. $^1\text{H NMR}$ (500 MHz, CDCl_3) δ 9.25–9.19 (m, 2H), 8.97–8.92 (m, 1H), 8.41 (d, $J = 8.5$ Hz, 1H), 7.74–7.67 (m, 1H), 7.62–7.58 (m, 1H), 4.05 (s, 3H). $^{13}\text{C NMR}$ (126 MHz, CDCl_3) δ 165.4, 129.8, 127.3, 126.6, 126.3, 121.6, 120.6, 120.2, 118.8, 113.6, 52.7, 51.1, 22.8 ppm. HRMS (EI): m/z calcd for $\text{C}_{15}\text{H}_9\text{N}_3\text{O}_4$, 295.0593 [M^{+}]; found 295.0594.

tert-Butyl 7-nitro-9-(trifluoromethyl)pyrido[2,1- α]isoindole-6-

carboxylate (3dCF). According to the general procedure *N*-(tert-butyloxycarbonylmethyl)pyridinium bromide (0.194 g, 1 mmol) and 4-chloro-3,5-dinitrobenzotrifluoride (0.270 g, 1 mmol) were reacted affording **3dCF** (0.030 g, 8%), as orange crystals. $R_f = 0.46$ (AcOEt/Hexane, 1:5); M.p. 225–227 °C. $^1\text{H NMR}$ (500 MHz, CDCl_3) δ 10.04 (d, $J = 7.1$ Hz, 1H), 8.63 (s, 1H), 8.30 (d, $J = 1.6$ Hz, 1H), 8.23 (d, $J = 1.5$ Hz, 1H), 7.60–7.53 (m, 1H), 7.45 (td, $J = 7.0, 1.4$ Hz, 1H), 1.64 (s, 9H). $^{13}\text{C NMR}$ (126 MHz, CDCl_3) δ 161.0, 141.7, 132.2, 128.0, 124.9, 124.2, 122.3, 121.3, 120.7, 120.5, 119.9, 119.4, 117.8, 106.4, 83.4, 28.4 ppm. HRMS (EI): m/z calcd for $\text{C}_{18}\text{H}_{15}\text{N}_2\text{O}_4\text{F}_3$, 380.0984 [M^+]; found 380.0988

tert-Butyl 9-cyano-7-nitropyrido[2,1- α]isoindole-6-

carboxylate (3dCN). According to the general procedure (condition B) *N*-(tert-butyloxycarbonylmethyl)pyridinium bromide (0.194 g, 1 mmol) and 4-chloro-3,5-dinitrobenzotrifluoride (0.227 g, 1 mmol) were reacted affording **3dCN** (0.299 g, 85%), as dark red crystals. $R_f = 0.65$ (AcOEt/Hexane, 1:1); M.p. 185–187 °C. $^1\text{H NMR}$ (500 MHz, CDCl_3) δ 10.02 (d, $J = 7.0$ Hz, 1H), 8.67 (d, $J = 1.3$ Hz, 1H), 8.30 (d, $J = 8.5$ Hz, 1H), 8.17 (d, $J = 1.3$ Hz, 1H), 7.62 (ddd, $J = 8.5, 7.0, 1.0$ Hz, 1H), 7.50 (ddd, $J = 7.0, 7.0, 1.3$ Hz, 1H), 1.63 (s, 9H). $^{13}\text{C NMR}$ (126 MHz, CDCl_3) δ 160.8, 141.5, 141.0, 132.0, 129.9, 128.2, 126.0, 125.2, 120.2, 120.1, 119.9, 118.2, 117.9, 100.8, 83.8, 28.4 ppm. HRMS (EI): m/z calcd for $\text{C}_{18}\text{H}_{15}\text{N}_3\text{O}_4$, 337.1063 [M^{+}]; found 337.1067.

6-(tert-Butyl) 9-methyl 7-nitropyrido[2,1- α]isoindole-6,9-

dicarboxylate (3dCO). According to the general procedure (condition B) *N*-(tert-butyloxycarbonylmethyl)pyridinium bromide (0.194 g, 1 mmol) and methyl 4-chloro-3,5-dinitrobenzoate (0.260 g, 1 mmol) were reacted affording **3dCO** (0.074 g, 20%) as orange crystals. $R_f = 0.64$ (AcOEt/Hexane, 1:1); M.p. 216–218 °C. $^1\text{H NMR}$ (500 MHz, CDCl_3) δ 10.01 (d, $J = 7.0$

Hz, 1H), 9.09 (d, *J* = 1.3 Hz, 1H), 8.63 (d, *J* = 1.4 Hz, 1H), 8.33 (d, *J* = 8.5 Hz, 1H), 7.59 – 7.53 (m, 1H), 7.46 – 7.41 (m, 1H), 4.01 (s, 3H), 1.64 (s, 9H). ¹³C NMR (126 MHz, CDCl₃) δ 165.9, 161.1, 141.2, 132.9, 128.1, 127.4, 125.1, 124.5, 121.2, 120.4, 120.3, 119.3, 117.9, 106.7, 83.3, 52.5, 28.4 ppm. HRMS (EI): *m/z* calcd for C₁₉H₁₈N₂O₆, 370.1165 [M⁺]; found 370.1164.

tert-Butyl 2-cyano-7-nitro-9-(trifluoromethyl)pyrido[2,1-*a*]isoindole-6-carboxylate (3eCF). According to the general procedure (condition B) 1-(2-(*tert*-butoxy)-2-oxoethyl)-4-cyanopyridin-1-ium chloride (0.219 g, 1 mmol) and 4-chloro-3,5-dinitrobenzotrifluoride (0.270 g, 1 mmol) were reacted affording **3eCF** (0.100 g, 25%), as orange crystals. *R_f* = 0.60 (AcOEt/Hexane, 1:1); M.p. 205-207°C. ¹H NMR (500 MHz, CDCl₃) δ 9.96 (dd, *J* = 7.4, 1.0 Hz, 1H), 8.70 (s, 1H), 8.65 – 8.63 (m, 1H), 8.29 (s, 1H), 7.52 (dd, *J* = 7.4, 1.9 Hz, 1H), 1.63 (s, 9H). ¹³C NMR (126 MHz, CDCl₃) δ 160.2, 142.4, 129.3, 127.4, 124.4, 123.4 (q, *J* = 34.4 Hz), 122.9, 122.01 (q, *J* = 4.1 Hz), 121.6 (q, *J* = 3.1 Hz), 120.9, 120.5, 119.2, 117.0, 110.0, 105.2, 84.9, 28.2 ppm. HRMS (EI): *m/z* calcd for C₁₉H₁₄F₃N₃O₄, 405.0936 [M⁺]; found 405.0950.

tert-Butyl 2,9-dicyano-7-nitropyrido[2,1-*a*]isoindole-6-carboxylate (3eCN). According to the general procedure (condition B) 1-(2-(*tert*-butoxy)-2-oxoethyl)-4-cyanopyridin-1-ium chloride (0.219 g, 1 mmol) and 4-chloro-3,5-dinitrobenzotrifluoride (0.227 g, 1 mmol) were reacted affording **3eCN** (0.089 g, 24%), as orange crystals. *R_f* = 0.65 (AcOEt/Hexane, 1:1); M.p. 340-342 °C. ¹H NMR (600 MHz, CDCl₃) δ 9.97 (d, *J* = 7.4 Hz, 1H), 8.75 (s, 1H), 8.63 (s, 1H), 8.25 (s, 1H), 7.55 (dd, *J* = 7.4, 1.9 Hz, 1H), 1.62 (s, 9H). ¹³C NMR (151 MHz, CDCl₃) δ 160.0, 142.3, 131.9, 129.7, 129.2, 127.6, 126.1, 122.9, 121.0, 120.2, 119.7, 117.3, 116.7, 106.1, 104.2, 85.3, 28.2 ppm. HRMS (APCI): *m/z* calcd for C₁₉H₁₄N₄O₄, 362.1015 [M⁺]; found 362.1021.

6-(tert-Butyl) 9-methyl 2-cyano-7-nitropyrido[2,1-*a*]isoindole-6,9-dicarboxylate (3eCO). According to the general procedure (condition B) 1-(2-(*tert*-butoxy)-2-oxoethyl)-4-cyanopyridin-1-ium chloride (0.219 g, 1 mmol) and methyl 4-chloro-3,5-dinitrobenzoate (0.260 g, 1 mmol) were reacted affording **3eCO** (0.026 g, 6%) as orange crystals. *R_f* = 0.62 (AcOEt/Hexane, 1:2); M.p. decomposed at 270°C; ¹H NMR (600 MHz, CDCl₃) δ 9.93 (d, *J* = 7.3 Hz, 1H), 9.14 (s, 1H), 8.70 (s, 1H), 8.65 (s, 1H), 7.50 (dd, *J* = 6.8, 1.1 Hz, 1H), 4.04 (s, 3H), 1.64 (s, 9H). ¹³C NMR (151 MHz, CDCl₃) δ 165.2, 160.3, 141.9, 129.9, 127.4, 126.9, 125.3, 123.2, 122.9, 121.3, 121.2, 119.1, 117.1, 110.2, 105.2, 84.8, 52.8, 28.2 ppm. HRMS (APCI): *m/z* calcd for C₂₀H₁₇N₃O₆, 395.1117 [M⁺]; found 395.1119.

6-(tert-Butyl) 9-methyl 2-(dimethylamino)-7-nitropyrido[2,1-*a*]isoindole-6,9-dicarboxylate (3fCO). According to the general procedure 1-(2-(*tert*-butoxy)-2-oxoethyl)-4-(dimethylamino)pyridin-1-ium chloride (0.237 g, 1 mmol) and methyl 4-chloro-3,5-dinitrobenzoate (0.260 g, 1 mmol) were reacted affording **3fCO** (0.053 g, 13%) as purple crystals. *R_f* =

0.55 (AcOEt/Hexane, 2:1); M.p. decomposed at 220°C. ¹H NMR (600 MHz, DMF-*d*₇) δ 9.71 (d, *J* = 7.8 Hz, 1H), 9.29 (d, *J* = 1.4 Hz, 1H), 8.41 (d, *J* = 1.4 Hz, 1H), 8.07 (d, *J* = 2.9 Hz, 1H), 7.33 (dd, *J* = 7.9, 2.9 Hz, 1H), 3.94 (s, 3H), 3.27 (s, 6H), 1.57 (s, 10H). ¹³C-NMR was not possible to record because of low solubility. HRMS (EI): *m/z* calcd for C₂₁H₂₃N₃O₆, 436.1485 [M+Na]⁺; found 436.1481.

Procedure for the synthesis of 7-Amino-9-(trifluoromethyl)pyrido[2,1-*a*]isoindole-6-carbonitrile (4). **3cCF** (0.170 g, 0.5 mmol) was dissolved in 3 mL of MeOH in a Schlenk tube under Argon flow. Pd/C (0.020 g, 0.18 mmol, 10%wt) and ammonium formate (0.250 g, 4 mmol) were added, and the resulting mixture was stirred for 24 h under inert atmosphere. When the reaction was complete (monitored by TLC), Pd/C was filtered off through a Celite pad using MeOH as eluent. The solvent was removed under reduced pressure and the crude product was purified by column chromatography (silica; AcOEt/Hexane, 3:7). Pale yellow crystals were obtained in the yield of 0.165 g, 60%. *R_f* = 0.60 (AcOEt/Hexane, 1:2); M.p. 205-206 °C. ¹H NMR (500 MHz, CDCl₃) δ 8.60 (d, *J* = 6.7 Hz, 1H), 8.13 (d, *J* = 8.5 Hz, 1H), 7.82 (s, 1H), 7.37 – 7.33 (m, 1H), 7.32 – 7.27 (m, 1H), 6.83 (s, 1H), 4.51 (s, 2H). ¹³C NMR (126 MHz, CDCl₃) δ 137.4, 132.0, 125.8, 125.5, 125.1, 123.5, 122.5, 118.9, 118.1, 117.4, 115.9 (q, *J* = 177 Hz), 107.8 (q, *J* = 4.8 Hz), 105.3 (q, *J* = 2.5 Hz), 84.8 ppm. HRMS (ESI): *m/z* calcd for C₁₄H₇F₃N₃, 274.0592 [M-H]⁻; found, 274.0583.

Procedure for the synthesis of 7-Nitropyrido[2,1-*a*]isoindole-9-carbonitrile (5). **3dCN** (0.240 g, 0.7 mmol) was dissolved in 3mL of DCM in a round bottom flask. A pipette of TFA was added, the mixture changed color from red to yellow and was stirred overnight at RT. When the reaction was complete (monitored by TLC), NaHCO₃ (aqueous solution) was added, and extraction was performed with AcOEt. Organic phases (purple) were collected, washed, and dried under vacuum. The product was purified by column chromatography (silica; AcOEt/Hexane, 3:7). A dark purple solid was obtained in the yield of 0.059 g 35%. *R_f* = 0.68 (AcOEt/Hexane, 3:7); M.p. 291-293 °C. ¹H NMR (600 MHz, CDCl₃) δ 8.76 (br s, 1H), 8.65 (d, *J* = 1.2 Hz, 1H), 8.53 (d, *J* = 6.7 Hz, 1H), 8.52 (s, 1H), 8.26 (d, *J* = 8.6 Hz, 1H), 7.42 – 7.37 (m, 1H), 7.37 – 7.32 (m, 1H). ¹³C NMR (126 MHz, CDCl₃) δ 137.0, 132.6, 129.6, 126.2, 125.9, 121.6, 120.0, 119.0, 118.9, 118.8, 106.7, 98.4 ppm. HRMS (EI): *m/z* calcd for C₁₃H₇N₃O₂, 237.0538 [M⁺]; found, 237.0546. HRMS (EI): *m/z* calcd for C₁₃H₇N₃O₂, 237.0538 [M⁺]; found, 237.0546.

Photophysical measurements

HPLC grade solvents were purchased from Sigma-Aldrich and used as obtained. For optical studies, solutions of molecules at low concentrations were used to avoid dimerization or reabsorption effects. All absorption and fluorescence spectra were taken at room temperature (21 °C). A Shimadzu UV/VIS-NIR spectrophotometer, model UV-3600i Plus, was used for absorption spectra measurement. Fluorescence spectra were recorded with an FS5 spectrofluorometer from Edinburgh Instruments. Fluorescence quantum yields (FQY) of molecules

in solvents at 21 °C were determined using Cumarin 153, 9,10-diphenylanthracene, Fluorescein and Sulforhodamine 101 as FQY standards. Solutions of low absorbance ($A < 0.1$) were used to avoid reabsorption or concentration quenching. Refractive index correction for solvents have been performed in the calculations of quantum yields. Molar absorption coefficient, ϵ , was calculated from the absorbance, A , of a solution of the given molar concentration, c , in a cuvette of length, l , according to Lambert-Beer formula: $A = c \times \epsilon \times l$.

Crystallography

X-ray diffraction data was collected at the Advanced Light Source (ALS), Lawrence Berkeley National Lab, Berkeley, CA, endstation 12.2.1 using a silicon monochromated beam of 17 KeV ($\lambda = 0.7288 \text{ \AA}$). A single crystal of **3bCN** was mounted on a MiTeGen 10 μm aperture Dual-Thickness MicroMount, and data collection was conducted at 100 K, with the crystal cooled by a stream of dry nitrogen. Bruker APEX3 software was used for data collection, Bruker SAINT V8.38A software was used to conduct the cell refinement and data reduction procedures, and absorption corrections were carried out utilizing the TWINABS program due to non-merohedral twinning.⁸² Initial structure solutions were found using direct methods (SHELXT),⁸³ and refinements were carried out using SHELXL-2014,⁸³ as implemented by Olex2.⁸⁴ Thermal parameters for all non-hydrogen atoms were refined anisotropically. Hydrogen atoms were placed in calculated positions and refined isotropically. The structure has been deposited to the Cambridge Crystallographic Data Centre (CCDC) under deposition number 2132628.

Computational details. We have started by performing DFT and TD-DFT calculations with the Gaussian 16 code⁸⁵ on all dyes. Default Gaussian16 thresholds and algorithms were used but for an improved optimization threshold (10^{-5} au on average residual forces), a stricter self-consistent field convergence criterion (10^{-10} a.u.) and the use of the *ultrafine* DFT integration grid. Firstly, the S_0 geometries have been optimized with DFT and the vibrational frequencies have been analytically determined, using the M06-2X *meta*-GGA hybrid exchange-correlation functional.⁸⁶ These calculations were performed with the 6-311G(d,p) atomic basis set and account for solvent effects through the Polarizable Continuum Model (PCM) approach considering DCM as solvent.⁸⁷ Secondly, starting from the optimal ground-state geometries, we have used TD-DFT with the same functional and basis set to optimize the S_1 geometry and compute the corresponding vibrational frequencies. All optimized structures are true minima of the potential energy surface (no imaginary frequency). Thirdly, the vertical transition energies were determined with TD-DFT and the same functional, but a larger basis set, namely 6-311+G(2d,p), in gas-phase as well as in solution using the recently-developed cLR² variant of the PCM,⁸⁸ in its *non-equilibrium* limit. As the shortcomings of TD-DFT for CT derivatives as well as for triplet energies are known, the transition energies were also computed using CC2⁸⁹ and SCS-CC2⁹⁰ with the Turbomole 7.3 code.⁹¹ The (SCS-)CC2 energies were calculated in gas phase applying the resolution of identity scheme, and using the *aug-cc-pVTZ* atomic basis set. Combining the CC2 and TD-DFT data using a well-known protocol,⁷³ one can obtain accurate CC2-corrected estimates of the

0-0 energies that can be straightforwardly compared to experimental values. Vertical absorption and emission energies were corrected in the same way. The reported S - T gaps are gas-phase SCS-CC2 values computed in the S_1 geometry, as SCS-CC2 is known to be exceptionally efficient for these gaps.⁹² The SOC matrix elements were determined at the M06-2X/*def2*-TZVP level using ORCA.5.0.1⁹³ with Dichloromethane as solvent was modelled with the SMD solvation model. The RIJCOSX method was used to accelerate the calculation and TightSCF settings were applied, whereas TDA was turned off. The SOC reported in the body of the text were determined as:

$$\sqrt{\frac{1}{3}S_x^2 + \frac{1}{3}S_y^2 + \frac{1}{3}S_z^2}$$

The vibronic couplings were determined with the FCClasses 3 program, on the basis of TD-DFT data.^{94,95} The radiative and internal conversion rates were obtained within the time-dependent formulation, the FC approach and the *Vertical Gradient* model,⁹⁶ thanks to the TVCF formalism of Peng and Shuai,⁷⁵ implemented in FCClasses by Cerezo and Santoro. For both the radiative and internal conversion rates, we used a 10 cm^{-1} broadening Gaussian, which is a typical value when modeling organic dyes.^{97,98}

Author Contributions

Conceptualization: D.T.G., J.S.A.B.; Investigation: J.S.A.B., B.K., M.H.E.B., E.T.O., D.J.; Supervision: D.T.G., D.J.; Visualization: J.S.A.B., D.J.; Writing – original draft: J.S.A.B., D.J.; D.T.G.; Writing – review & editing: D.T.G., B.K., J.S.A.B., D.J., E.T.O.

Conflicts of interest

There are no conflicts to declare.

Acknowledgements

The work was financially supported by the Polish National Science Centre, Poland (HARMONIA 2018/30/M/ST5/00460), the Foundation for Polish Science (TEAM POIR.04.04.00-00-3CF4/16-00). This project received funding from European Union's Horizon 2020 research and innovation programme under Grant Agreement No 860762. M.H.E.B. and D.J. thank the CCIPL computational center installed in Nantes for generous allocation of computational time. We extend our gratitude to Dr. Simon J. Teat for training and guidance through our crystallography studies at the Advanced Light Source (ALS), Lawrence Berkeley National Laboratory, supported by the Office of Science, Office of Basic Energy Sciences, of the U.S. Department of Energy under Contract No. DE-AC02-05CH11231.

Notes and references

- 1 A. E. Tschitschibabin, Tautomerie in der Pyridin-Reihe, *Berichte Dtsch. Chem. Ges. B Ser.*, 1927, **60**, 1607–1617.

- 2 A. Angeli, Ueber die Einwirkung des Oxaldiäthylesters auf das Pyrrolmethylketon, *Berichte Dtsch. Chem. Ges.*, 1890, **23**, 1793–1797.
- 3 A. Angeli, Ueber die Einwirkung des Oxaldiäthylesters auf das Pyrrolmethylketon, *Berichte Dtsch. Chem. Ges.*, 1890, **23**, 2154–2160.
- 4 A. Angeli, *Gazzetta Chimica Italiana*, 1890.
- 5 E. Kim, Y. Lee, S. Lee and S. B. Park, Discovery, Understanding, and Bioapplication of Organic Fluorophore: A Case Study with an Indolizine-Based Novel Fluorophore, Seoul-Fluor, *Acc. Chem. Res.*, 2015, **48**, 538–547.
- 6 R. Ji, A. Liu, S. Shen, X. Cao, F. Li and Y. Ge, An indolizine–rhodamine based FRET fluorescence sensor for highly sensitive and selective detection of Hg²⁺ in living cells, *RSC Adv.*, 2017, **7**, 40829–40833.
- 7 H. Sonnenschein, G. Hennrich, U. Resch-Genger and B. Schulz, Fluorescence and UV/Vis spectroscopic behaviour of novel biindolizines, *Dyes Pigments*, 2000, **46**, 23–27.
- 8 A. J. Huckaba, A. Yella, L. E. McNamara, A. E. Steen, J. S. Murphy, C. A. Carpenter, G. D. Punecky, N. I. Hammer, M. K. Nazeeruddin, M. Grätzel and J. H. Delcamp, Molecular Design Principles for Near-Infrared Absorbing and Emitting Indolizine Dyes, *Chem. – Eur. J.*, 2016, **22**, 15536–15542.
- 9 J. Wan, C.-J. Zheng, M.-K. Fung, X.-K. Liu, C.-S. Lee and X.-H. Zhang, Multifunctional electron-transporting indolizine derivatives for highly efficient blue fluorescence, orange phosphorescence host and two-color based white OLEDs, *J. Mater. Chem.*, 2012, **22**, 4502.
- 10 B. Koszarna, R. Matczak, M. Krzeszewski, O. Vakuliuk, J. Klajn, M. Tasior, J. T. Nowicki and D. T. Gryko, Direct arylation of electron-poor indolizines, *Tetrahedron*, 2014, **70**, 225–231.
- 11 G. Martinez-Ariza, B. T. Mehari, L. A. G. Pinho, C. Foley, K. Day, J. C. Jewett and C. Hulme, Synthesis of fluorescent heterocycles via a Knoevenagel/[4 + 1]-cycloaddition cascade using acetyl cyanide, *Org. Biomol. Chem.*, 2017, **15**, 6076–6079.
- 12 D. Chernyak, C. Skontos and V. Gevorgyan, Two-Component Approach Toward a Fully Substituted N-Fused Pyrrole Ring, *Org. Lett.*, 2010, **12**, 3242–3245.
- 13 R.-R. Liu, C.-J. Lu, M.-D. Zhang, J.-R. Gao and Y.-X. Jia, Palladium-Catalyzed Three-Component Cascade Reaction: Facial Access to Densely Functionalized Indolizines, *Chem. Eur. J.*, 2015, **21**, 7057–7060.
- 14 M. Kucukdisli and T. Opatz, One-Pot Synthesis of Polysubstituted Indolizines by an Addition/Cycloaromatization Sequence, *J. Org. Chem.*, 2013, **78**, 6670–6676.
- 15 J. Barluenga, G. Lonzi, L. Riesgo, L. A. López and M. Tomás, Pyridine Activation via Copper(I)-Catalyzed Annulation toward Indolizines, *J. Am. Chem. Soc.*, 2010, **132**, 13200–13202.
- 16 H. Zhu, N. Shao, T. Chen and H. Zou, Functionalized heterocyclic scaffolds derived from Morita–Baylis–Hillman Acetates, *Chem. Commun.*, 2013, **49**, 7738.
- 17 D. Coffinier, L. El Kaim and L. Grimaud, Nef-Perkow Access to Indolizine Derivatives, *Synlett*, 2010, **2010**, 2474–2476.
- 18 T. Xu and H. Alper, Synthesis of Indolizine Derivatives by Pd-Catalyzed Oxidative Carbonylation, *Org. Lett.*, 2015, **17**, 4526–4529.
- 19 S. Chuprakov, F. W. Hwang and V. Gevorgyan, Rh-Catalyzed Transannulation of Pyridotriazoles with Alkynes and Nitriles, *Angew. Chem. Int. Ed.*, 2007, **46**, 4757–4759.
- 20 B. Sadowski, J. Klajn and D. T. Gryko, Recent advances in the synthesis of indolizines and their π -expanded analogues, *Org. Biomol. Chem.*, 2016, **14**, 7804–7828.
- 21 T. Uchida and K. Matsumoto, Methods for the Construction of the Indolizine Nucleus, *Synthesis*, 1976, 209–236.
- 22 F. J. Swinbourne, J. H. Hunt and G. Klinkert, in *Advances in Heterocyclic Chemistry*, Elsevier, 1979, vol. 23, pp. 103–170.
- 23 N. S. Prostavok and O. B. Baktibaev, Indolizines, *Russ. Chem. Rev.*, 1975, **44**, 748.
- 24 H. L. Blewitt, in *Chemistry of Heterocyclic Compounds*, John Wiley & Sons, Ltd, 1977, pp. 117–178.
- 25 D. Basavaiah, B. Devendar, D. Lenin and T. Satyanarayana, The Baylis–Hillman Bromides as Versatile Synthons: A Facile One-Pot Synthesis of Indolizine and Benzofused Indolizine Frameworks, *Synlett*, 2009, 411–416.
- 26 B. Yan and Y. Liu, Gold-Catalyzed Multicomponent Synthesis of Aminoindolizines from Aldehydes, Amines, and Alkynes under Solvent-Free Conditions or in Water, *Org. Lett.*, 2007, **9**, 4323–4326.
- 27 Ss. S. Patil, S. V. Patil and V. D. Bobade, Synthesis of Aminoindolizine and Quinoline Derivatives via Fe(acac)₃/TBA-OH-Catalyzed Sequential Cross-Coupling–Cycloisomerization Reactions, *N. Y.*, 2011, 5.
- 28 Y. Yang, C. Xie, Y. Xie and Y. Zhang, Synthesis of Functionalized Indolizines via Copper-Catalyzed Annulation of 2-Alkylazaarenes with α,β -Unsaturated Carboxylic Acids, *Org. Lett.*, 2012, **14**, 957–959.
- 29 C. Feng, Y. Yan, Z. Zhang, K. Xu and Z. Wang, Cerium(III)-catalyzed cascade cyclization: an efficient approach to functionalized pyrrolo[1,2-a]quinolines, *Org. Biomol. Chem.*, 2014, **12**, 4837–4840.
- 30 Z. Li, D. Chernyak and V. Gevorgyan, Palladium-Catalyzed Carbonylative Cyclization/Arylation Cascade for 2-Aroylindolizine Synthesis, *Org. Lett.*, 2012, **14**, 6056–6059.
- 31 R.-R. Liu, Z.-Y. Cai, C.-J. Lu, S.-C. Ye, B. Xiang, J. Gao and Y.-X. Jia, Indolizine synthesis via Cu-catalyzed cyclization of 2-(2-enynyl)pyridines with nucleophiles, *Org. Chem. Front.*, 2015, **2**, 226–230.
- 32 K.-S. Lee, T.-K. Kim, J. H. Lee, H.-J. Kim and J.-I. Hong, Fluorescence turn-on probe for homocysteine and cysteine in water, *Chem. Commun.*, 2008, 6173.
- 33 X. Wang, S. Li, Y. Pan, H. Wang, H. Liang, Z. Chen and X. Qin, Samarium(III)-Catalyzed C(sp³)-H Bond Activation: Synthesis of Indolizines via C–C and C–N Coupling between 2-Alkylazaarenes and Propargylic Alcohols, *Org. Lett.*, 2014, **16**, 580–583.
- 34 X. Meng, P. Liao, J. Liu and X. Bi, Silver-catalyzed cyclization of 2-pyridyl alkynyl carbinols with isocyanides: divergent synthesis of indolizines and pyrroles, *Chem Commun*, 2014, **50**, 11837–11839.
- 35 M. Nayak and I. Kim, Construction of benzo-fused indolizines, pyrrolo[1,2-a]quinolines via alkyne–carbonyl metathesis, *Org. Biomol. Chem.*, 2015, **13**, 9697–9708.
- 36 E. M. Roberts, M. Gates and V. Boekelheide, A SYNTHESIS OF 5,6-BENZOPYRROCOLINE ³, *J. Org. Chem.*, 1955, **20**, 1443–1447.
- 37 J. Liu, L. Zhou, W. Ye and C. Wang, Formal [3+2] cycloaddition of 1-cyanocyclopropane 1-ester with pyridine, quinoline or isoquinoline: a general and efficient strategy for construction of cyanoindolizine skeletons, *Chem Commun*, 2014, **50**, 9068–9071.
- 38 D. Basavaiah, G. Veeraraghavaiah and S. S. Badsara, Ketones as electrophiles in two component Baylis–Hillman reaction: a facile one-pot synthesis of substituted indolizines, *Org. Biomol. Chem.*, 2014, **12**, 1551.
- 39 J. Bricoché, C. Meyer and J. Cossy, Synthesis of 2-Aminoindolizines by 1,3-Dipolar Cycloaddition of Pyridinium Ylides with Electron-Deficient Ynamides, *Org. Lett.*, 2015, **17**, 2800–2803.

- 40 I. V. Seregin and V. Gevorgyan, Gold-Catalyzed 1,2-Migration of Silicon, Tin, and Germanium en Route to C-2 Substituted Fused Pyrrole-Containing Heterocycles, *J. Am. Chem. Soc.*, 2006, **128**, 12050–12051.
- 41 B. Sahoo, M. N. Hopkinson and F. Glorius, External-Photocatalyst-Free Visible-Light-Mediated Synthesis of Indolizines, *Angew. Chem. Int. Ed.*, 2015, **54**, 15545–15549.
- 42 S. Park and I. Kim, Electron-withdrawing group effect in aryl group of allyl bromides for the successful synthesis of indolizines via a novel [3+3] annulation approach, *Tetrahedron*, 2015, **71**, 1982–1991.
- 43 W. Hao, H. Wang, Q. Ye, W.-X. Zhang and Z. Xi, Cyclopentadiene-Phosphine/Palladium-Catalyzed Synthesis of Indolizines from Pyrrole and 1,4-Dibromo-1,3-butadienes, *Org. Lett.*, 2015, **17**, 5674–5677.
- 44 S. G. Dawande, B. S. Lad, S. Prajapati and S. Katukojvala, Rhodium-catalyzed pyridannulation of indoles with diazoenals: a direct approach to pyrido[1,2-*a*]indoles, *Org. Biomol. Chem.*, 2016, **14**, 5569–5573.
- 45 Y. Jung and I. Kim, Deformylative Intramolecular Hydroarylation: Synthesis of Benzo[*e*]pyrido[1,2-*a*]indoles, *Org. Lett.*, 2015, **17**, 4600–4603.
- 46 Y. Jung and I. Kim, Synthesis of 6-Aryl-5-iodobenzo[*e*]pyrido[1,2-*a*]indoles by 6-endo-dig Iodocyclization, *Asian J. Org. Chem.*, 2016, **5**, 147–152.
- 47 L. Dalton and T. Teitei, Synthesis of Benz[*b*]indolizines and related compounds, *Aust. J. Chem.*, 1969, **22**, 1525.
- 48 F. D. Saeva and H. R. Luss, Novel synthesis of the 2,3-benzindolizine ring system. Mechanism of formation, redox, electronic absorption, and fluorescence behavior, *J. Org. Chem.*, 1988, **53**, 1804–1806.
- 49 A. Fozard and C. K. Bradsher, Synthesis of the pyrido[2,1-*a*]isoindole system by an intramolecular photochemical cyclization, *J. Org. Chem.*, 1967, **32**, 2966–2969.
- 50 C. K. Bradsher and C. F. Voigt, Electrophilic substitution of the pyrido[2,1-*a*]isoindole system, *J. Org. Chem.*, 1971, **36**, 1603–1607.
- 51 S. Kajigaeshi, S. Mori, S. Fujisaki and S. Kanemasa, *exo*-Selective Peripheral Cycloaddition Reactions of Pyrido[2,1-*a*]isoindole, *Bull. Chem. Soc. Jpn.*, 1985, **58**, 3547–3551.
- 52 W. Augstein and F. Kröhnke, Synthesen des Benzo[*a*]- und des Naphtho[2.3-*b*]indolizin-Ringsystems, *Justus Liebigs Ann. Chem.*, 1966, **697**, 158–170.
- 53 C. C. Chintawar, M. V. Mane, A. G. Tathe, S. Biswas and N. T. Patil, Gold-Catalyzed Cycloisomerization of Pyridine-Bridged 1,8-Diynes: An Expedient Access to Luminescent Cycl[3.2.2]azines, *Org. Lett.*, 2019, **21**, 7109–7113.
- 54 B. Zhao, M. Yu, H. Liu, Y. Chen, Y. Yuan and X. Xie, Rhodium-Catalyzed Direct Oxidative C-H Acylation of 2-Arylpyridines with Terminal Alkynes: A Synthesis of Pyrido[2,1-*a*]isoindoles, *Adv. Synth. Catal.*, 2014, **356**, 3295–3301.
- 55 C. Xie, Y. Zhang and P. Xu, Novel Synthesis of Pyrido[2,1-*a*]isoindoles via a Three-Component Assembly Involving Benzynes, *Synlett*, 2008, 3115–3120.
- 56 T. Mitsumori, M. Bendikov, O. Dautel, F. Wudl, T. Shioya, H. Sato and Y. Sato, Synthesis and Properties of Highly Fluorescent Indolizino[3,4,5-*ab*]isoindoles, *J. Am. Chem. Soc.*, 2004, **126**, 16793–16803.
- 57 S. Asako, T. Kobashi and K. Takai, Use of Cyclopropane as C1 Synthetic Unit by Directed Retro-Cyclopropanation with Ethylene Release, *J. Am. Chem. Soc.*, 2018, **140**, 15425–15429.
- 58 X. Chen, X. Hu, Y. Deng, H. Jiang and W. Zeng, A [4 + 1] Cyclative Capture Access to Indolizines via Cobalt(III)-Catalyzed Csp²-H Bond Functionalization, *Org. Lett.*, 2016, **18**, 4742–4745.
- 59 X. Huang and T. Zhang, Multicomponent reactions of pyridines, α -bromo carbonyl compounds and silylaryl triflates as arylene precursors: a facile one-pot synthesis of pyrido[2,1-*a*]isoindoles, *Tetrahedron Lett.*, 2009, **50**, 208–211.
- 60 T.-J. Gong, M.-Y. Xu, S.-H. Yu, C.-G. Yu, W. Su, X. Lu, B. Xiao and Y. Fu, Rhodium(III)-Catalyzed Directed C-H Coupling with Methyl Trifluoroacrylate: Diverse Synthesis of Fluoroalkenes and Heterocycles, *Org. Lett.*, 2018, **20**, 570–573.
- 61 S. Liu, X. Li and J. Cheng, Facile Synthesis of Pyrido[2,1-*a*]isoindoles via Iron-Mediated 2-Arylpyridine C-H Bond Cleavage, *N. Y.*, 2013, 5.
- 62 B. Valeur, *Molecular Fluorescence: Principles and Applications*, Wiley, 1st edn., 2001.
- 63 D. Reuschling and F. Kröhnke, Ringschlüsse unter HNO₂-Abspaltung und C-C-Verknüpfung, II. Synthese neuer Ringsysteme, *Chem. Ber.*, 1971, **104**, 2103–2109.
- 64 E. Stefănescu and M. Petrovanu, [(*p*. tolyl)-pyridazinium-ylides. (VII). Action of picryl chlorides and chloranil on 3-(*p*. tolyl)-pyridazine-phenacylide], *Rev. Med. Chir. Soc. Med. Nat. Iasi*, 1977, **81**, 475–478.
- 65 S.-W. Liu, Y.-J. Gao, Y. Shi, L. Zhou, X. Tang and H.-L. Cui, Synthesis of Benzoindolizines through 1,5-Electrocyclization/Oxidation Cascades, *J. Org. Chem.*, 2018, **83**, 13754–13764.
- 66 E. C. Taylor and I. J. Turchi, 1,5-Dipolar cyclizations, *Chem. Rev.*, 1979, **79**, 181–231.
- 67 M.-C. Chen, D.-G. Chen and P.-T. Chou, Fluorescent Chromophores Containing the Nitro Group: Relatively Unexplored Emissive Properties, *ChemPlusChem*, 2021, **86**, 11–27.
- 68 W. Rodríguez-Córdoba, L. Gutiérrez-Arzaluz, F. Cortés-Guzmán and J. Peon, Excited state dynamics and photochemistry of nitroaromatic compounds, *Chem. Commun.*, 2021, **57**, 12218–12235.
- 69 S. Ram and R. E. Ehrenkauf, A general procedure for mild and rapid reduction of aliphatic and aromatic nitro compounds using ammonium formate as a catalytic hydrogen transfer agent, *Tetrahedron Lett.*, 1984, **25**, 3415–3418.
- 70 P. H. Gore, The Friedel-Crafts Acylation Reaction and its Application to Polycyclic Aromatic Hydrocarbons, *Chem. Rev.*, 1955, **55**, 229–281.
- 71 Y. Tominaga, Y. Shiroshita, Y. Matsuda and A. Hosomi, ChemInform Abstract: The Effect of Benzannelation Toward Cycl[3.2.2]azine. Synthesis and Physical Properties of Dibenzo(*a,h*)cycl[3.2.2]azine., *ChemInform*.
- 72 S. M. McDonald, S. K. Møllerup, C. Barran, X. Wang and S. Wang, Binding Modes and Reactivity of Pyrido[2,1-*a*]isoindole as a Neutral Carbon Donor with Main-Group and Transition-Metal Elements, *Organometallics*, 2017, **36**, 4054–4060.
- 73 D. Jacquemin, I. Duchemin and X. Blase, 0–0 Energies Using Hybrid Schemes: Benchmarks of TD-DFT, CIS(D), ADC(2), CC2, and BSE/ GW formalisms for 80 Real-Life Compounds, *J. Chem. Theory Comput.*, 2015, **11**, 5340–5359.
- 74 T. Le Bahers, C. Adamo and I. Ciofini, A Qualitative Index of Spatial Extent in Charge-Transfer Excitations, *J. Chem. Theory Comput.*, 2011, **7**, 2498–2506.
- 75 Q. Peng, Y. Yi, Z. Shuai and J. Shao, Excited state radiationless decay process with Duschinsky rotation effect: Formalism and implementation, *J. Chem. Phys.*, 2007, **126**, 114302.

- 76 K. M. Elattar, I. Youssef and A. A. Fadda, Reactivity of indolizines in organic synthesis, *Synth. Commun.*, 2016, **46**, 719–744.
- 77 D. He, Y. Xu, J. Han, H. Deng, M. Shao, J. Chen, H. Zhang and W. Cao, Facile one-pot tandem synthesis of perfluoroalkylated indolizines under metal-free mild conditions, *Tetrahedron*, 2017, **73**, 938–944.
- 78 L. G. Voskressensky, A. A. Festa, E. A. Sokolova and A. V. Varlamov, Synthesis of chromeno[2',3':4,5]imidazo[2,1-a]isoquinolines via a novel domino reaction of isoquinoline-derived immonium salts. Scope and limitations, *Tetrahedron*, 2012, **68**, 5498–5504.
- 79 M. Costa, A. I. Rodrigues and F. Proença, Synthesis of 3-aminochromenes: the Zincke reaction revisited, *Tetrahedron*, 2014, **70**, 4869–4875.
- 80 P. N. Praveen Rao, M. Amini, H. Li, A. G. Habeeb and E. E. Knaus, Design, Synthesis, and Biological Evaluation of 6-Substituted-3-(4-methanesulfonylphenyl)-4-phenylpyran-2-ones: A Novel Class of Diarylheterocyclic Selective Cyclooxygenase-2 Inhibitors, *J. Med. Chem.*, 2003, **46**, 4872–4882.
- 81 A. T. Nielsen, W. P. Norris, R. L. Atkins and W. R. Vuono, Nitrocarbons. 3. Synthesis of decanitrobiphenyl, *J. Org. Chem.*, 1983, **48**, 1056–1059.
- 82 APEX3, SAINT, and TWINABS. Bruker AXS. Madison, WI, USA, .
- 83 G. M. Sheldrick, SHELXT – Integrated space-group and crystal-structure determination, *Acta Crystallogr. Sect. Found. Adv.*, 2015, **71**, 3–8.
- 84 O. V. Dolomanov, L. J. Bourhis, R. J. Gildea, J. a. K. Howard and H. Puschmann, OLEX2: a complete structure solution, refinement and analysis program, *J. Appl. Crystallogr.*, 2009, **42**, 339–341.
- 85 M. J. Frisch, et al., *Gaussian 16, revision A.03; Gaussian Inc.: Wallingford, CT, 2016*, .
- 86 Y. Zhao and D. G. Truhlar, The M06 suite of density functionals for main group thermochemistry, thermochemical kinetics, noncovalent interactions, excited states, and transition elements: two new functionals and systematic testing of four M06-class functionals and 12 other functionals, *Theor. Chem. Acc.*, 2008, **120**, 215–241.
- 87 J. Tomasi, B. Mennucci and R. Cammi, Quantum Mechanical Continuum Solvation Models, *Chem. Rev.*, 2005, **105**, 2999–3094.
- 88 C. A. Guido, A. Chrayteh, G. Scalmani, B. Mennucci and D. Jacquemin, Simple Protocol for Capturing Both Linear-Response and State-Specific Effects in Excited-State Calculations with Continuum Solvation Models, *J. Chem. Theory Comput.*, 2021, **17**, 5155–5164.
- 89 O. Christiansen, H. Koch and P. Jørgensen, The second-order approximate coupled cluster singles and doubles model CC2, *Chem. Phys. Lett.*, 1995, **243**, 409–418.
- 90 C. Hättig, A. Hellweg and A. Köhn, Distributed memory parallel implementation of energies and gradients for second-order Møller–Plesset perturbation theory with the resolution-of-the-identity approximation, *Phys. Chem. Chem. Phys.*, 2006, **8**, 1159.
- 91 TURBOMOLE V7.3, a development of University of Karlsruhe and Forschungszentrum Karlsruhe GmbH, 1989–2007; TURBOMOLE GmbH, .
- 92 A. Pershin, D. Hall, V. Lemaire, J.-C. Sancho-Garcia, L. Muccioli, E. Zysman-Colman, D. Beljonne and Y. Olivier, Highly emissive excitons with reduced exchange energy in thermally activated delayed fluorescent molecules, *Nat. Commun.*, 2019, **10**, 597.
- 93 F. Neese, F. Wennmohs, U. Becker and C. Riplinger, The ORCA quantum chemistry program package, *J. Chem. Phys.*, 2020, **152**, 224108.
- 94 J. Cerezo, F. Santoro, FCClasses 3.0, <http://www.pi.iccom.cnr.it/fcclasses>.
- 95 F. Santoro, R. Improta, A. Lami, J. Bloino and V. Barone, Effective method to compute Franck-Condon integrals for optical spectra of large molecules in solution, *J. Chem. Phys.*, 2007, **126**, 084509.
- 96 F. Santoro and D. Jacquemin, Going beyond the vertical approximation with time-dependent density functional theory: Going beyond the vertical approximation with TD-DFT, *Wiley Interdiscip. Rev. Comput. Mol. Sci.*, 2016, **6**, 460–486.
- 97 A. Humeniuk, M. Bužančić, J. Hoče, J. Cerezo, R. Mitrić, F. Santoro and V. Bonačić-Koutecký, Predicting fluorescence quantum yields for molecules in solution: A critical assessment of the harmonic approximation and the choice of the lineshape function, *J. Chem. Phys.*, 2020, **152**, 054107.
- 98 Q. Ou, Q. Peng and Z. Shuai, Toward Quantitative Prediction of Fluorescence Quantum Efficiency by Combining Direct Vibrational Conversion and Surface Crossing: BODIPYs as an Example, *J. Phys. Chem. Lett.*, 2020, **11**, 7790–7797.